Magnetic reconnection on dayside crustal magnetic fields at Mars: MAVEN observations

Y. Harada[1], J. S. Halekas[1], G. A. DiBraccio[2], S. Xu[3], J. Espley[2], J. P. McFadden[3], D. L. Mitchell[3], C. Mazelle[4], D. A. Brain[5], T. Hara[3], Y. J. Ma[6], S. Ruhunusiri[1], and B. M. Jakosky[5]

Yuki Harada, yuki-harada@uiowa.edu

[1]Department of Physics and Astronomy, University of Iowa, Iowa City, IA, USA

[2]NASA Goddard Space Flight Center, Greenbelt, MD, USA

[3]Space Sciences Laboratory, University of California, Berkeley, CA, USA

[4]IRAP, University of Toulouse, CNRS, UPS, CNES, Toulouse, France

[5]Laboratory for Atmospheric and Space Physics, University of Colorado, Boulder, CO, USA

This article has been accepted for publication and undergone full peer review but has not been through the copyediting, typesetting, pagination and proofreading process, which may lead to differences between this version and the Version of Record. Please cite this article as doi: 10.1002/2018GL077281

The identification of magnetic reconnection on the dayside of Mars has been elusive owing to the lack of comprehensive plasma and field measurements. Here we present direct measurements of dayside in-situ reconnection signatures by the comprehensive particles and fields package onboard the Mars Atmosphere and Volatile EvolutioN (MAVEN) spacecraft over strong crustal magnetic fields in the southern hemisphere of Mars. During a crossing of a bifurcated current sheet consisting of northward and southward magnetic fields, MAVEN recorded (i) ionospheric photoelectrons trapped on closed magnetic field lines, (ii) Hall magnetic fields and a nonzero normal field with polarity consistent with a crossing northward of the X line, and (iii) northward Alfvénic ion jets. Dayside magnetic reconnection on crustal magnetic fields could control the global configuration and topology of the Martian magnetosphere and alter the ion escape pattern from the dayside ionosphere.

Keypoints:

- First comprehensive evidence for in-situ magnetic reconnection signatures over crustal magnetic fields on the dayside of Mars
- Observed signatures include closed magnetic topology, Hall and normal magnetic fields, and ion jets within a bifurcated current sheet

[6]Institute of Geophysics and Planetary Physics, UCLA, Los Angeles, CA, USA

- Dayside reconnection could control the global magnetospheric configuration and dayside ion escape pathways

1. Introduction

Magnetic reconnection on the dayside magnetopause plays a fundamental role in the dynamics of the terrestrial magnetosphere [*Dungey*, 1961]. Meanwhile, it remains elusive whether magnetic reconnection operates on the dayside of Mars, and if so, how it dictates the structure and dynamics of the Martian magnetosphere. As summarized by *Halekas et al.* [2009], current sheets capable of reconnection can be generated on the dayside of Mars in multiple possible configurations: (i) between the interplanetary magnetic field (IMF) on both sides (equivalent cases are considered for comets and Venus [*Niedner and Brandt*, 1978; *Vech et al.*, 2016]), (ii) between the IMF on one side and crustal field on the other [*Krymskii et al.*, 2002; *Hara et al.*, 2014, 2016], and (iii) between the crustal field on both sides [*Brain et al.*, 2010; *Beharrell and Wild*, 2012]. Though effects and products of dayside reconnection at Mars have been discussed in the aforementioned literature, there have been few reports on direct measurements of in-situ reconnection signatures (such as accelerated plasma flows and Hall magnetic fields within current sheets [e.g., *Paschmann et al.*, 2013]). *Halekas et al.* [2009] conducted a systematic search for Hall magnetic field signatures detected by Mars Global Surveyor (MGS) at 400 km altitude and identified 26 Hall field events, only one of which was observed on the dayside (at solar zenith angles less than 70 degrees). For the lone dayside event, no conclusive characterization of particle distributions could be made due to noisy electron distributions and the lack of ion measurements. To our knowledge, no comprehensive and definitive measurements of ion, electron, and magnetic field signatures of dayside magnetic reconnection at Mars have been reported, and the identification of dayside reconnection remains inconclusive.

This paper reports on the first comprehensive measurements of in-situ reconnection signatures on the dayside of Mars from the Mars Atmosphere and Volatile EvolutioN (MAVEN) mission [*Jakosky et al.*, 2015]. We utilize electron measurements by the Solar Wind Electron Analyzer (SWEA) instrument [*Mitchell et al.*, 2016], ion measurements by the SupraThermal And Thermal Ion Composition (STATIC) instrument [*McFadden et al.*, 2015], and magnetic field measurements by the Magnetometer (MAG) [*Connerney et al.*, 2015]. The reconnection event was observed on 6 October 2016, when MAVEN traversed strong crustal magnetic fields in the southern hemisphere. We first present MAVEN observations of the reconnection event and then discuss implications for the global configuration of the Martian magnetosphere and ion escape from Mars.

2. Observations

Figures 1a–1d present the orbital configuration of MAVEN during 18:03–18:12 UT on 6 October 2016 in Mars Solar Orbital (MSO) coordinates, in which X points from Mars toward the Sun, Y points opposite to the direction of Mars' orbital velocity component perpendicular to X, and Z completes the orthogonal coordinate set. During this time interval, MAVEN traveled through the dayside magnetic pileup region (MPR), which represents the plasma region dominated by planetary ions with elevated magnetic field magnitudes [*Nagy et al.*, 2004], below the nominal magnetic pileup boundary (Figure 1b) from the dawn side to the dusk side in the southern hemisphere (Figures 1a, 1c, and 1d). As shown in the geographic projection (Figure 1e), MAVEN's orbit passed over strong crustal magnetic fields in the southern hemisphere of Mars.

Figure 2 shows a time series of particles and fields data obtained by MAVEN during 18:03–18:12 UT on 6 October 2016. MAVEN crossed a current sheet at 18:07:15 UT as characterized by a rapid rotation of the magnetic field from northward $+B_z$ to southward $-B_z$ accompanied by a decrease in the magnetic field magnitude (labeled as "CS" in Figure 2g). The northward magnetic field ($+B_z$) before the current sheet crossing is either a magnetic field of crustal origin or a draped magnetic field of solar wind origin. As the direction of draped IMF was variable within the magnetosheath and MPR before this time interval (not shown), it is difficult to estimate the instantaneous upstream IMF direction and see if it is consistent with the local magnetic field direction. After the current sheet crossing, the measured magnetic field polarity is consistent with that of the crustal field computed from the spherical harmonic model [*Morschhauser et al.*, 2014] (dashed lines in Figure 2g) and the measured and crustal fields show similar variations with an offset in B_z. This suggests that the magnetic field after the current sheet crossing contains a significant contribution from the crustal origin, presumably compressed by the upstream plasma. The shear angle between the magnetic fields on the two sides is $\sim$142°.

Figures 2a–2c show electron measurements around the current sheet crossing, which can be utilized to infer magnetic field topology with respect to the electron exobase at $\sim$160–220 km altitudes. Based on the electron energy spectra and pitch angle distributions, we identify four regions with different characteristics bounded by the magenta dashed lines in Figures 2a–2c.

In the first region (labeled "1. draped/open" in Figure 2), MAVEN observed a large flux of hot electrons at $\sim$100–1000 eV (Figure 2a) with nearly isotropic distributions within

the measured pitch angle range (Figure 2b). Figure 2c show the pitch angle-resolved shape parameter derived from 20–80 eV electron distributions [*Xu et al.*, 2017a], which is designed in such a way that small values <1 indicate that electrons traveling in a particular direction are dominated by ionospheric photoelectrons. The direction of electrons relative to the planet ("Towards"/"Away") is determined based on the local magnetic field direction. The shape parameter shows large values (>∼1) in the "Towards" direction (Figure 2c), indicating solar wind origin of the measured electrons, while the "Away" shape parameter cannot be obtained because of the gaps in the antiparallel direction (the white regions in Figure 2b). From these measurements, we infer magnetic topology of either draped field lines with both ends connected to the solar wind (solar wind electrons traveling in both directions) or open field lines with the antiparallel end connected to the solar wind and the parallel end to the collisional atmosphere (parallel solar wind electrons and unmeasured ionospheric electrons in the antiparallel gaps). This situation is illustrated by the northward field line labeled "1. draped/open" in Figure 1f. The fate of the parallel end is ambiguous, either connected to the collisional atmosphere or draped around the planet without intersecting the photoelectron source.

In the second region (labeled "2. closed" in Figure 2), the 100–1000 eV electron flux decreases and the electron energy spectra exhibit characteristic features of ionospheric photoelectrons (Figure 2a) with a peak at 22–27 eV, sharp decrease at 60–70 eV, ∼500 eV Auger electron peak, and another sharp decrease just above the Auger peak [*Xu et al.*, 2017a]. The small shape parameters <1 in both directions (Figure 2c) indicate that ionospheric photoelectrons are supplied from both ends of closed field lines connected

to the dayside collisional atmosphere as illustrated by the line labeled "2. closed" in Figure 1f. We note that the field line connection to the collisional atmosphere inferred from electron measurements does not necessarily guarantee the connection to the crustal source.

In the third region (labeled "3. open" in Figure 2), the hot electron pitch angle distributions display loss cones in the parallel direction (Figure 2b). The shape parameters show large values $\sim$1 for "Towards" electrons and small values $<$1 for "Away" electrons (Figure 2c). These observations suggest open field lines on which ionospheric photoelectrons are supplied from the antiparallel end and solar wind electrons precipitate from the parallel end as illustrated by the southward line labeled "3. open" in Figure 1f.

In the fourth region (labeled "4. closed" in Figure 2), we observe energy spectra characteristic of ionospheric photoelectrons (Figure 2a). The shape parameters exhibit small values $<$1 in both directions (except for the "Away" gaps), suggesting closed field line topology with both ends connected to the dayside collisional atmosphere as illustrated by the line labeled "4. closed" in Figure 1f.

We now look at magnetic field signatures. Figure 3a shows magnetic field components in the current sheet LMN coordinate system derived from the minimum variance analysis (MVA) [*Sonnerup and Cahill*, 1967; *Sonnerup and Scheible*, 1998] of magnetic fields during 18:06:38–18:08:00 UT (indicated by the vertical dashed lines in Figures 2e–2h and 3). In the LMN system, L is along the antiparallel magnetic fields (corresponding to the maximum variance direction), M is along the X line (intermediate variance direction), and N is along the current sheet normal (minimum variance direction). The obtained eigen-

value ratios are large (>10), implying that the LMN system is well determined. The B_{L} profile exhibits a two-step variation (a bifurcated current sheet), which is a characteristic signature of a Petschek-type reconnection exhaust [e.g., *Hoshino et al.*, 1996; *Gosling et al.*, 2005]. We observe a bipolar variation in B_{M} (labeled "Hall B") and a non-zero B_{N} component of -8 nT (labeled "Normal B") as expected for a crossing of a reconnecting current sheet around the ion diffusion region [*Halekas et al.*, 2009; *Paschmann et al.*, 2013]. The polarity of the Hall magnetic field is consistent with a crossing northward of the X line as illustrated in Figure 1f. The observed $|B_{\mathrm{N}}/B_{\mathrm{L}}| \sim 0.2$ is roughly consistent with those observed around the terminator and in the nightside magnetotail [*Halekas et al.*, 2009; *Harada et al.*, 2017]. Under the assumption that the current sheet is stationary, we obtain a current sheet thickness of ∼162 km from the crossing time (∼45 s, see Figure 2g) and the normal component of the spacecraft velocity (3.6 km/s). Ion measurements around the current sheet indicate the normal velocity components of $V_{\mathrm{N}} \sim -8$ km/s for H^+, ~ -1 km/s for O^+, and ~ 0 km/s for O_2^+ ions (not shown). Assuming that the current sheet moves with protons, the relative spacecraft velocity of ∼11.6 km/s implies a current sheet thickness of ∼522 km.

Finally we investigate ion measurements. Figures 2d, 2e, and 2f show the ion energy spectra, ion densities, and ion bulk velocities, respectively. The most abundant ion species is O_2^+ throughout the interval (Figure 2e), indicating the predominance of planetary plasma in the MPR. Based on the measured ion pressures and magnetic field magnitude, we obtain the plasma beta (the ratio of plasma pressure to magnetic pressure) of $\beta \sim 0.29$ (0.26) immediately before (after) the current sheet crossing. The low β

indicates the dominant magnetic pressure as expected in the MPR [e.g., *Ma et al.*, 2004]. Coinciding with the magnetic field rotation from the northward $+B_z$ to southward $-B_z$, we observe northward turning of the proton flow in the V_z component (labeled as "jet" in Figure 2f). The northward flow is opposite to southward flows nominally expected in the southern hemisphere (diverging plasma flows from the subsolar point toward the flank). Figures 3b–3d show the V_L component of H^+, O^+, and O_2^+ ions. The northward jets ($+V_L$ deviation) are seen during the current sheet crossing for all the ions species. The heavier species display smaller V_L changes (∼13 km/s for H^+, ∼3 km/s for O^+, and ∼2 km/s for O_2^+ ions), suggesting that these ions are still unmagnetized and their motions are controlled mostly by electric fields, as is the case for reconnection events observed in the nightside magnetotail [*Harada et al.*, 2015, 2017]. Based on the ion densities in the current sheet, we obtain the ion inertial lengths of 43 km for H^+, 65 km for O^+, and 52 km for O_2^+, which imply the estimated local half thickness of the current sheet (∼81–261 km) is of the order of ∼1–6 ion inertial lengths. In such a thin current sheet, the ions are expected to be mostly unmagnetized. The observed V_L changes are roughly on the same order of, or slightly smaller than, the Alfvén speed of ∼10 km/s derived from the total ion mass density in the regions adjacent to the current sheet (Figure 2h). We note that though a fluid in an idealized reconnection exhaust is expected to be accelerated eventually up to approximately the Alfvén speed from a magnetohydrodynamic perspective [e.g., *Yamada et al.*, 2010], individual species may have different outflow speeds at a particular location depending on their different stages of acceleration and remagnetization as well as on the individual Alfvén speeds [e.g., *Markidis et al.*, 2011; *Liu et al.*, 2015]. For the dominant

O_2^+ ions, we also derive high time resolution velocity data from the three dimensional data product without mass resolution by assuming that all ions are O_2^+ (shown by the red line in Figure 3d). The red line closely follows the black line, demonstrating the validity of the assumption, and clearly resolves the jet structure with a V_L peak near the center of the current sheet. The northward Alfvénic ion jets within the current sheet is consistent with a crossing northward of the X line as illustrated in Figure 1f.

To ensure that the variations in the computed ion velocity moments do not arise from instrumental effects caused by the incomplete field of view (FOV) of STATIC [*McFadden et al.*, 2015], we examine ion angular spectra in the instrument coordinates (Figure 4). During this time interval, the $+X_{\mathrm{STATIC}}$, $+Y_{\mathrm{STATIC}}$, and $+Z_{\mathrm{STATIC}}$ directions were nearly aligned with $-Y_{\mathrm{MSO}}$, $+Z_{\mathrm{MSO}}$, and $-X_{\mathrm{MSO}}$, respectively. Note that [phi, theta] = [0°, 0°] corresponds to $-Y_{\mathrm{MSO}}$ and [+90°, 0°] corresponds to $+Z_{\mathrm{MSO}}$. The elevation angle spectra (Figures 4b, 4d, and 4f) display generally broad distributions with bulk velocity directions (solid white lines) well within the FOV (±45°) during the current sheet crossing. In Figures 4a, 4c, and 4e, the azimuthal angle spectra exhibit ion flow rotations (indicated by the white arrows) corresponding to the $+V_L$ jets (Figures 3b–3d). For O^+ and O_2^+ ions (Figures 4c and 4e), the main populations are observed apart from the anodes at 67.5–90°, the look directions of which were partially blocked by the spacecraft body at this time, indicating that the ion jets were detected in the clear part of the FOV. Meanwhile, the H^+ jet population could be partially blocked, but this blockage would result in a slightly smaller rotation in the bulk velocity (Figure 4a), suggesting a possible underestimation of the H^+ jet velocity. Therefore, we conclude that the ion jets measured during the current

sheet crossing are not artificial changes in the computed velocity moments caused by the limited FOV.

3. Implications

As illustrated in Figure 1f, MAVEN observed magnetic reconnection signatures during a current sheet crossing above strong crustal magnetic fields on the dayside of Mars, including (i) closed magnetic field lines containing ionospheric photoelectrons travelling in both parallel and antiparallel directions, (ii) Hall magnetic fields and a nonzero normal field in the bifurcated current sheet with polarity consistent with a crossing northward of the X line, and (iii) northward Alfvénic ion jets with lower flow velocities for heavier ion species. The Hall magnetic fields, which arise from differential motion between unmagnetized ions and magnetized electrons, indicate the presence of a thin current sheet with a thickness of the order of ion inertial lengths, which is confirmed by the ion measurements. This thin current sheet is presumably generated by interaction between the compressed crustal fields and upstream plasma with magnetic fields at a large shear angle. The formation of a thin current sheet is a necessary condition for collisonless reconnection [*Sanny et al.*, 1994; *Phan et al.*, 2010], and the magnetic shear angle of 142° and $\Delta\beta \sim 0.03$ suggest that reconnection is allowed for this current sheet according to the condition of *Swisdak et al.* [2010]. All of the observed signatures (the polarity of Hall and nonzero normal fields, northward ion jets, and closed topology current sheet) consistently suggest the spacecraft crossing northward of the X line. The comprehensiveness and consistency of the observed signatures within the current sheet strongly suggest the occurrence of magnetic reconnection on dayside crustal magnetic fields.

Although the origin of the northward magnetic field before the current sheet crossing has not been uniquely identified, the crustal magnetic fields are most likely implicated in the southward magnetic field on the other side of the current sheet, given the consistent polarity and variation of the measured and model fields. Therefore, this event can involve magnetic reconnection between either (i) the draped IMF and crustal magnetic field or (ii) crustal fields on both sides. In the former case of IMF-crustal field reconnection, the field-line connection of the parallel end to the collisional atmosphere in the "closed" topology would not represent the connection to the crustal source. Instead, the field lines in the parallel direction should eventually drape around the planet, threading through the collisional atmosphere. In the latter case of internal reconnection between crustal magnetic fields, the closed magnetic topology during the current sheet crossing would truly represent magnetic field lines with both ends connected to the Martian surface.

In either case, the comprehensive evidence for dayside magnetic reconnection presented in this paper has an important implication: magnetic reconnection can operate in realistic plasma parameters around dayside crustal magnetic fields at Mars. Dayside reconnection between the IMF and crustal fields could account for the distorted magnetic field configuration observed by MGS on the dayside [*Brain et al.*, 2006; *Luhmann et al.*, 2015a]. *Luhmann et al.* [2015b] proposed that much of the nightside magnetotail of Mars could be composed of open and closed field lines with at least one end connected to the planet, which presumably result from magnetic reconnection. Data-model comparison on the Martian magnetotail configuration suggests that the Martian magnetosphere has hybrid nature of induced and intrinsic magnetospheres [*DiBraccio et al., The Twisted Configuration of the*

Martian Magnetotail: MAVEN Observations, submitted to Geophys. Res. Lett., 2018]. In this "hybrid magnetosphere" model, dayside magnetic reconnection between the IMF and crustal magnetic fields partially controls the nightside magnetotail configuration as opposed to a purely induced magnetotail configuration that is determined solely by the draped IMF. Dayside magnetic reconnection, the occurrence of which is demonstrated by the comprehensive in-situ measurements by MAVEN, could have a global consequence in the topology and configuration of the Martian magnetosphere.

Dayside magnetic reconnection can also alter the ion escape pattern from the dayside ionosphere by changing magnetic field topology [*Luhmann et al.*, 2017]. Open field lines provide pathways on which planetary ions can be accelerated and escape into space [*Ergun et al.*, 2006; *Frahm et al.*, 2010; *Dubinin et al.*, 2012; *Lillis et al.*, 2015, 2017], whereas closed field lines can trap ionospheric plasma [*Brain et al.*, 2007; *Andrews et al.*, 2015; *Flynn et al.*, 2017; *Xu et al.*, 2017b]. As magnetic reconnection can switch open field lines to closed field lines, and vice versa, magnetic reconnection on dayside crustal magnetic fields can play an important role in regulating escape channels from a major reservoir of planetary ions, that is, the dayside ionosphere. An important next step would be quantitative evaluation of the roles of dayside reconnection in modifying the magnetospheric configuration and ion escape pattern. Future studies should investigate the occurrence rate and spatial distribution of the dayside magnetic reconnection by conducting a systematic search for in-situ reconnection signatures.

Acknowledgments. MAVEN data are publicly available through the Planetary Data System at https://pds-ppi.igpp.ucla.edu.

References

Andrews, D. J., L. Andersson, G. T. Delory, R. E. Ergun, A. I. Eriksson, C. M. Fowler, T. McEnulty, M. W. Morooka, T. Weber, and B. M. Jakosky (2015), Ionospheric plasma density variations observed at Mars by MAVEN/LPW, *Geophys. Res. Lett.*, *42*(21), 8862–8869, doi:10.1002/2015GL065241.

Beharrell, M. J., and J. A. Wild (2012), Stationary flux ropes at the southern terminator of Mars, *J. Geophys. Res.*, *117*(A12), A12,212, doi:10.1029/2012JA017738.

Brain, D. A., D. L. Mitchell, and J. S. Halekas (2006), The magnetic field draping direction at Mars from April 1999 through August 2004, *Icarus*, *182*(2), 464 – 473, doi: 10.1016/j.icarus.2005.09.023, results from the Mars Express ASPERA-3 Investigation.

Brain, D. A., A. H. Baker, J. Briggs, J. P. Eastwood, J. S. Halekas, and T.-D. Phan (2010), Episodic detachment of Martian crustal magnetic fields leading to bulk atmospheric plasma escape, *Geophys. Res. Lett.*, *37*(14), L14,108, doi:10.1029/2010GL043916.

Brain, D. A., R. J. Lillis, D. L. Mitchell, J. S. Halekas, and R. P. Lin (2007), Electron pitch angle distributions as indicators of magnetic field topology near Mars, *J. Geophys. Res.*, *112*(A9), A09,201, doi:10.1029/2007JA012435.

Connerney, J., J. Espley, P. Lawton, S. Murphy, J. Odom, R. Oliversen, and D. Sheppard (2015), The MAVEN Magnetic Field Investigation, *Space Sci. Rev.*, pp. 1–35, doi:10.1007/s11214-015-0169-4.

Dubinin, E., M. Fraenz, A. Fedorov, R. Lundin, N. Edberg, F. Duru, and O. Vaisberg (2012), Ion Energization and Escape on Mars and Venus, *Space Sci. Rev.*, *162*, 173–211, doi:10.1007/978-1-4614-3290-6_6.

Dungey, J. W. (1961), Interplanetary Magnetic Field and the Auroral Zones, *Phys. Rev. Lett.*, *6*, 47–48, doi:10.1103/PhysRevLett.6.47.

Ergun, R. E., L. Andersson, W. K. Peterson, D. Brain, G. T. Delory, D. L. Mitchell, R. P. Lin, and A. W. Yau (2006), Role of Plasma Waves in Mars' Atmospheric Loss, *Geophys. Res. Lett.*, *33*, L14,103, doi:10.1029/2006GL025785.

Flynn, C. L., M. F. Vogt, P. Withers, L. Andersson, S. England, and G. Liu (2017), MAVEN Observations of the Effects of Crustal Magnetic Fields on Electron Density and Temperature in the Martian Dayside Ionosphere, *Geophys. Res. Lett.*, *44*(21), 10,812–10,821, doi:10.1002/2017GL075367.

Frahm, R., J. Sharber, J. Winningham, R. Link, M. Liemohn, J. Kozyra, A. Coates, D. Linder, S. Barabash, R. Lundin, and A. Fedorov (2010), Estimation of the escape of photoelectrons from Mars in 2004 liberated by the ionization of carbon dioxide and atomic oxygen , *Icarus*, *206*(1), 50 – 63, doi:10.1016/j.icarus.2009.03.024.

Gosling, J. T., R. M. Skoug, D. J. McComas, and C. W. Smith (2005), Direct evidence for magnetic reconnection in the solar wind near 1 AU, *J. Geophys. Res.*, *110*(A1), A01,107, doi:10.1029/2004JA010809.

Halekas, J. S., J. P. Eastwood, D. A. Brain, T. D. Phan, M. Oieroset, and R. P. Lin (2009), In situ observations of reconnection Hall magnetic fields at Mars: Evidence for ion diffusion region encounters, *J. Geophys. Res.*, *114*, A11,204, doi:10.1029/2009JA014544.

Hara, T., K. Seki, H. Hasegawa, D. A. Brain, K. Matsunaga, M. H. Saito, and D. Shiota (2014), Formation processes of flux ropes downstream from Martian crustal magnetic fields inferred from Grad-Shafranov reconstruction, *J. Geophys. Res.*, *119*(9), 7947–

7962, doi:10.1002/2014JA019943.

Hara, T., D. A. Brain, D. L. Mitchell, J. G. Luhmann, K. Seki, H. Hasegawa, J. P. McFadden, J. S. Halekas, J. R. Espley, Y. Harada, R. Livi, G. A. DiBraccio, J. E. P. Connerney, C. Mazelle, L. Andersson, and B. M. Jakosky (2016), MAVEN observations of a giant ionospheric flux rope near Mars resulting from interaction between the crustal and interplanetary draped magnetic fields, *J. Geophys. Res.*, *121*, 828–842, doi:10.1002/2016JA023347.

Harada, Y., J. S. Halekas, J. P. McFadden, D. L. Mitchell, C. Mazelle, J. E. P. Connerney, J. Espley, D. E. Larson, D. A. Brain, L. Andersson, G. A. DiBraccio, G. A. Collinson, R. Livi, T. Hara, S. Ruhunusiri, and B. M. Jakosky (2015), Magnetic reconnection in the near-Mars magnetotail: MAVEN observations, *Geophys. Res. Lett.*, *42*, 8838–8845, doi:10.1002/2015GL065004.

Harada, Y., J. S. Halekas, J. P. McFadden, J. Espley, G. A. DiBraccio, D. L. Mitchell, C. Mazelle, D. A. Brain, L. Andersson, Y. J. Ma, D. E. Larson, S. Xu, T. Hara, S. Ruhunusiri, R. Livi, and B. M. Jakosky (2017), Survey of magnetic reconnection signatures in the Martian magnetotail with MAVEN, *J. Geophys. Res.*, *122*, doi:10.1002/2017JA023952.

Hoshino, M., A. Nishida, T. Mukai, Y. Saito, T. Yamamoto, and S. Kokubun (1996), Structure of plasma sheet in magnetotail: Double-peaked electric current sheet, *J. Geophys. Res.*, *101*(A11), 24,775–24,786, doi:10.1029/96JA02313.

Jakosky, B. M., R. P. Lin, J. M. Grebowsky, J. G. Luhmann, D. F. Mitchell, G. Beutelschies, T. Priser, M. Acuna, L. Andersson, D. Baird, D. Baker, R. Bartlett, M. Benna,

S. Bougher, D. Brain, D. Carson, S. Cauffman, P. Chamberlin, J.-Y. Chaufray, O. Cheatom, J. Clarke, J. Connerney, T. Cravens, D. Curtis, G. Delory, S. Demcak, A. DeWolfe, F. Eparvier, R. Ergun, A. Eriksson, J. Espley, X. Fang, D. Folta, J. Fox, C. Gomez-Rosa, S. Habenicht, J. Halekas, G. Holsclaw, M. Houghton, R. Howard, M. Jarosz, N. Jedrich, M. Johnson, W. Kasprzak, M. Kelley, T. King, M. Lankton, D. Larson, F. Leblanc, F. Lefevre, R. Lillis, P. Mahaffy, C. Mazelle, W. McClintock, J. McFadden, D. L. Mitchell, F. Montmessin, J. Morrissey, W. Peterson, W. Possel, J. A. Sauvaud, N. Schneider, W. Sidney, S. Sparacino, A. I. F. Stewart, R. Tolson, D. Toublanc, C. Waters, T. Woods, R. Yelle, and R. Zurek (2015), The Mars Atmosphere and Volatile Evolution (MAVEN) Mission, *Space Sci. Rev.*, doi:10.1007/s11214-015-0139-x.

Krymskii, A. M., T. K. Breus, N. F. Ness, M. H. Acuña, J. E. P. Connerney, D. H. Crider, D. L. Mitchell, and S. J. Bauer (2002), Structure of the magnetic field fluxes connected with crustal magnetization and topside ionosphere at Mars, *J. Geophys. Res.*, *107*(A9), 1245, doi:10.1029/2001JA000239.

Lillis, R. J., D. A. Brain, S. W. Bougher, F. Leblanc, J. G. Luhmann, B. M. Jakosky, R. Modolo, J. Fox, J. Deighan, X. Fang, Y. C. Wang, Y. Lee, C. Dong, Y. Ma, T. Cravens, L. Andersson, S. M. Curry, N. Schneider, M. Combi, I. Stewart, J. Clarke, J. Grebowsky, D. L. Mitchell, R. Yelle, A. F. Nagy, D. Baker, and R. P. Lin (2015), Characterizing Atmospheric Escape from Mars Today and Through Time, with MAVEN, *Space Sci. Rev.*, *195*(1), 357–422, doi:10.1007/s11214-015-0165-8.

Lillis, R. J., J. S. Halekas, M. O. Fillingim, A. R. Poppe, G. Collinson, D. A. Brain, and D. L. Mitchell (2017), Field-aligned electrostatic potentials above the Martian exobase

from MGS electron reflectometry: structure and variability, *J. Geophys. Res.*, *122*, doi:10.1002/2017JE005395.

Liu, Y. H., C. G. Mouikis, L. M. Kistler, S. Wang, V. Roytershteyn, and H. Karimabadi (2015), The heavy ion diffusion region in magnetic reconnection in the Earth's magnetotail, *J. Geophys. Res.*, *120*, 3535–3551, doi:10.1002/2015JA020982.

Luhmann, J., Y.-J. Ma, D. Brain, D. Ulusen, R. Lillis, J. Halekas, and J. Espley (2015a), Solar wind interaction effects on the magnetic fields around Mars: Consequences for interplanetary and crustal field measurements, *Planet. Space Sci.*, *117*, 15 – 23, doi: 10.1016/j.pss.2015.05.004.

Luhmann, J. G., C. Dong, Y. Ma, S. M. Curry, D. Mitchell, J. Espley, J. Connerney, J. Halekas, D. A. Brain, B. M. Jakosky, and C. Mazelle (2015b), Implications of MAVEN Mars near-wake measurements and models, *Geophys. Res. Lett.*, *42*(21), 9087–9094, doi: 10.1002/2015GL066122.

Luhmann, J. G., C. F. Dong, Y. J. Ma, S. M. Curry, S. Xu, C. O. Lee, T. Hara, J. Halekas, Y. Li, J. R. Gruesbeck, J. Espley, D. A. Brain, C. T. Russell, and B. M. Jakosky (2017), Martian magnetic storms, *J. Geophys. Res.*, *122*, doi:10.1002/2016JA023513.

Ma, Y., A. F. Nagy, I. V. Sokolov, and K. C. Hansen (2004), Three-dimensional, multispecies, high spatial resolution MHD studies of the solar wind interaction with Mars, *J. Geophys. Res.*, *109*(A7), A07,211, doi:10.1029/2003JA010367.

Markidis, S., G. Lapenta, L. Bettarini, M. Goldman, D. Newman, and L. Andersson (2011), Kinetic simulations of magnetic reconnection in presence of a background O+ population, *J. Geophys. Res.*, *116*(A1), A00K16, doi:10.1029/2011JA016429.

McFadden, J. P., O. Kortmann, D. Curtis, G. Dalton, G. Johnson, R. Abiad, R. Sterling, K. Hatch, P. Berg, C. Tiu, D. Gordon, S. Heavner, M. Robinson, M. Marckwordt, R. Lin, and B. Jakosky (2015), MAVEN SupraThermal and Thermal Ion Compostion (STATIC) Instrument, *Space Sci. Rev.*, *195*(1-4), 199–256, doi:10.1007/s11214-015-0175-6.

Mitchell, D. L., C. Mazelle, J.-A. Sauvaud, J.-J. Thocaven, J. Rouzaud, A. Fedorov, P. Rouger, D. Toublanc, E. Taylor, D. Gordon, M. Robinson, S. Heavner, P. Turin, M. Diaz-Aguado, D. W. Curtis, R. P. Lin, and B. M. Jakosky (2016), The MAVEN Solar Wind Electron Analyzer, *Space Sci. Rev.*, pp. 1–34, doi:10.1007/s11214-015-0232-1.

Morschhauser, A., V. Lesur, and M. Grott (2014), A spherical harmonic model of the lithospheric magnetic field of Mars, *J. Geophys. Res.*, *119*(6), 1162–1188, doi: 10.1002/2013JE004555.

Nagy, A., D. Winterhalter, K. Sauer, T. Cravens, S. Brecht, C. Mazelle, D. Crider, E. Kallio, A. Zakharov, E. Dubinin, M. Verigin, G. Kotova, W. Axford, C. Bertucci, and J. Trotignon (2004), The plasma environment of Mars, *Space Sci. Rev.*, *111*(1-2), 33–114, doi:10.1023/B:SPAC.0000032718.47512.92.

Niedner, M. B., Jr., and J. C. Brandt (1978), Interplanetary gas. XXII - Plasma tail disconnection events in comets - Evidence for magnetic field line reconnection at interplanetary sector boundaries, *Ap. J.*, *223*, 655–670, doi:10.1086/156299.

Paschmann, G., M. Øieroset, and T. Phan (2013), In-Situ Observations of Reconnection in Space, *Space Sci. Rev.*, *178*(2-4), 385–417, doi:10.1007/s11214-012-9957-2.

Phan, T. D., J. T. Gosling, G. Paschmann, C. Pasma, J. F. Drake, M. Øieroset, D. Larson, R. P. Lin, and M. S. Davis (2010), The Dependence of Magnetic Reconnection on Plasma and Magnetic Shear: Evidence from Solar Wind Observations, *Ap. J.*, *719*(2), L199, doi:10.1088/2041-8205/719/L199.

Sanny, J., R. L. McPherron, C. T. Russell, D. N. Baker, T. I. Pulkkinen, and A. Nishida (1994), Growth-phase thinning of the near-Earth current sheet during the CDAW 6 substorm, *J. Geophys. Res.*, *99*(A4), 5805–5816, doi:10.1029/93JA03235.

Sonnerup, B. U. Ö., and L. J. Cahill (1967), Magnetopause structure and attitude from Explorer 12 observations, *J. Geophys. Res.*, *72*(1), 171–183, doi:10.1029/JZ072i001p00171.

Sonnerup, B. U. Ö., and M. Scheible (1998), Minimum and Maximum Variance Analysis, *ISSI Scientific Reports Series*, *1*, 185–220.

Swisdak, M., M. Opher, J. F. Drake, and F. A. Bibi (2010), The Vector Direction of the Interstellar Magnetic Field Outside the Heliosphere, *Ap. J.*, *710*(2), 1769, doi: 10.1088/0004-637X/710/1769.

Trotignon, J., C. Mazelle, C. Bertucci, and M. Acuña (2006), Martian shock and magnetic pile-up boundary positions and shapes determined from the Phobos 2 and Mars Global Surveyor data sets , *Planet. Space Sci.*, *54*(4), 357 – 369, doi:10.1016/j.pss.2006.01.003.

Vech, D., G. Stenberg, H. Nilsson, N. J. T. Edberg, A. Opitz, K. Szegő, T. Zhang, and Y. Futaana (2016), Statistical features of the global polarity reversal of the Venusian induced magnetosphere in response to the polarity change in interplanetary magnetic field, *J. Geophys. Res.*, *121*, doi:10.1002/2015JA021995.

Xu, S., D. Mitchell, M. Liemohn, X. Fang, Y. Ma, J. Luhmann, D. Brain, M. Steckiewicz, C. Mazelle, J. Connerney, and B. Jakosky (2017a), Martian low-altitude magnetic topology deduced from MAVEN/SWEA observations, *J. Geophys. Res.*, *122*(2), 1831–1852, doi:10.1002/2016JA023467.

Xu, S., D. Mitchell, J. Luhmann, Y. Ma, X. Fang, Y. Harada, T. Hara, D. Brain, T. Weber, C. Mazelle, and G. A. DiBraccio (2017b), High-Altitude Closed Magnetic Loops at Mars Observed by MAVEN, *Geophys. Res. Lett.*, *44*(22), 11,229–11,238, doi: 10.1002/2017GL075831.

Yamada, M., R. Kulsrud, and H. Ji (2010), Magnetic reconnection, *Rev. Mod. Phys.*, *82*, 603–664, doi:10.1103/RevModPhys.82.603.

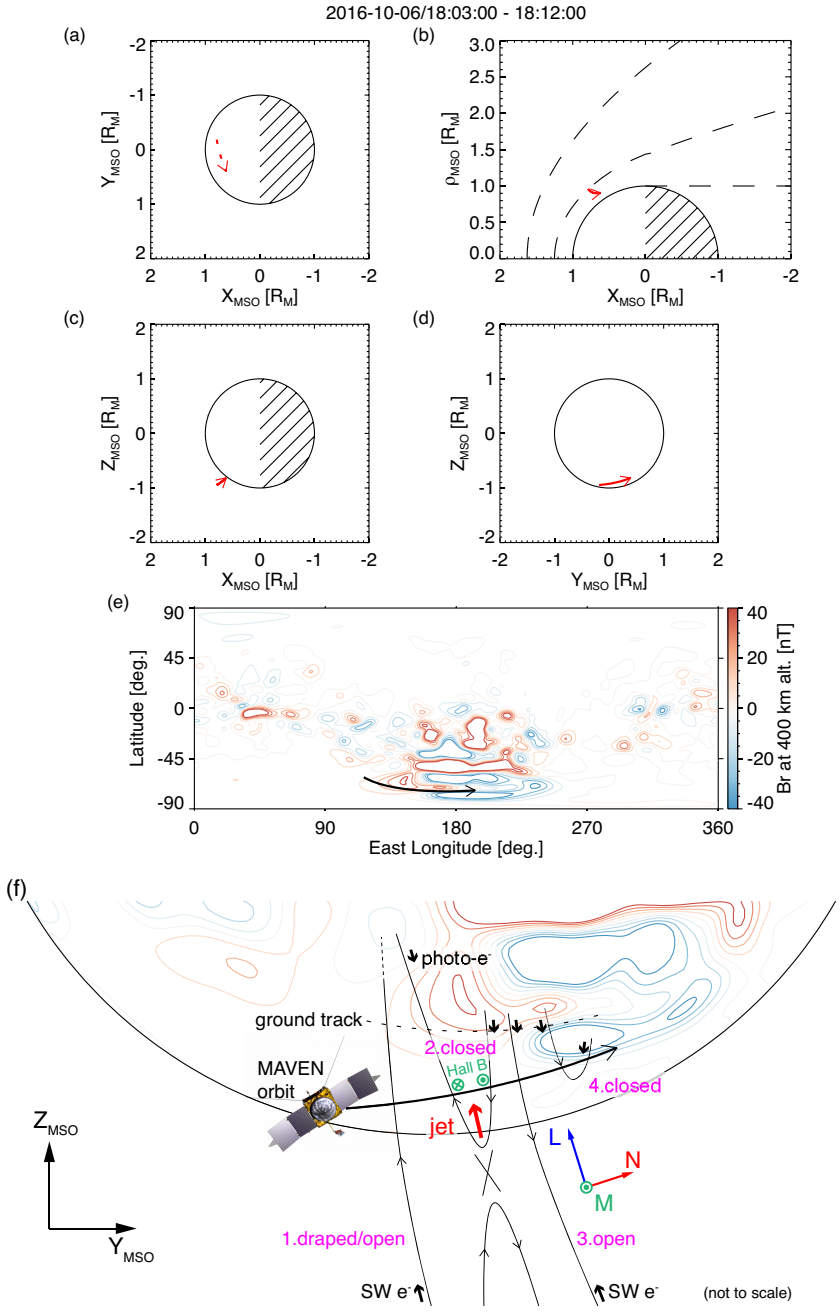

Figure 1. MAVEN orbit projection during 18:03–18:12 UT on 6 October 2016 on the (a) X_{MSO}–Y_{MSO}, (b) X_{MSO}–ρ_{MSO}, where $\rho_{\mathrm{MSO}} \equiv \sqrt{Y_{\mathrm{MSO}}^2 + Z_{\mathrm{MSO}}^2}$, (c) X_{MSO}–Z_{MSO}, (d) Y_{MSO}–Z_{MSO} planes, and (e) in geographic coordinates. The dashed arrow in Figure 1a indicates that the orbit is located on the $-Z_{\mathrm{MSO}}$ side of Mars. The dashed lines in Figure 1b represent the nominal positions of the bow shock and magnetic pileup boundary [*Trotignon et al.*, 2006] and the geometrical shadow boundary. The red and blue contours in Figure 1e show the radial component (positive outward) of crustal magnetic fields at a 400 km altitude computed from the spherical harmonic model [*Morschhauser et al.*, 2014]. (f) Schematic illustration of MAVEN crossing of magnetic reconnection structure above dayside crustal magnetic fields on 6 October 2016.

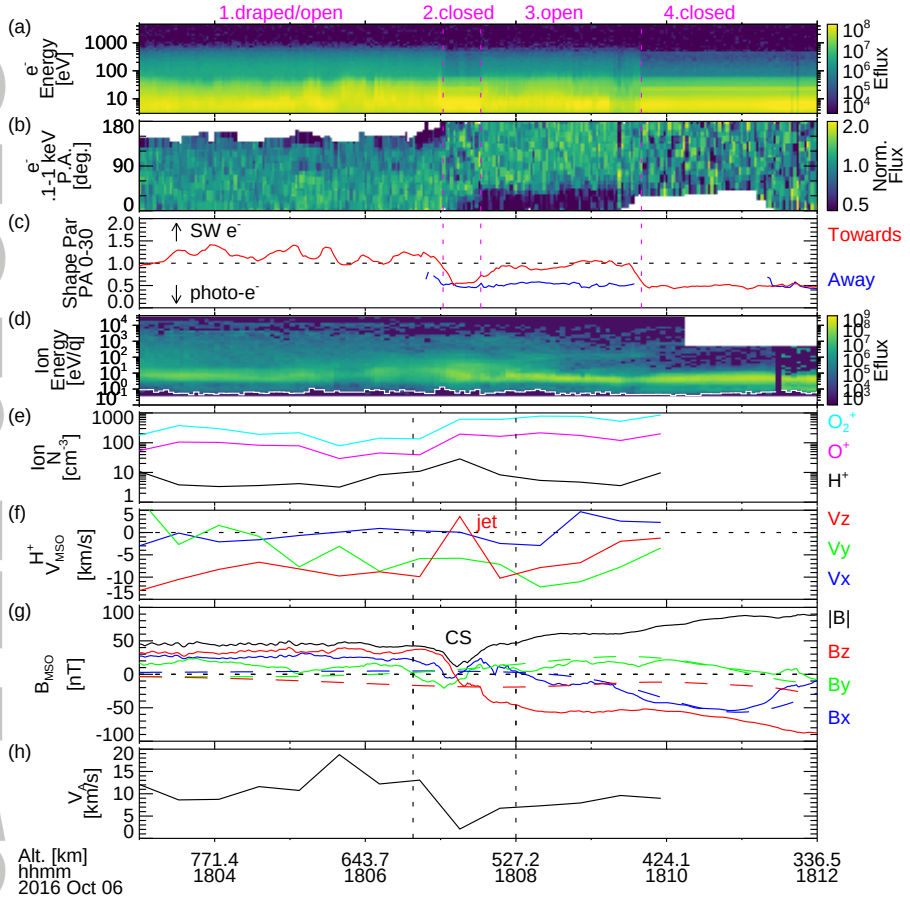

Figure 2. MAVEN observations during 18:03–18:12 UT on 6 October 2016 of (a) electron energy spectra in units of differential energy flux (Eflux) of eV/cm^2/s/st/eV and (b) pitch angle distributions of 100–1000 eV electrons in normalized flux, (c) pitch angle-resolved shape parameter [*Xu et al.*, 2017a], (d) ion energy spectra, (e) ion densities, (f) proton bulk velocity, (g) magnetic field in MSO coordinates, and (h) Alfvén speed computed from the total ion mass density. The white line in Figure 2d indicates the low-energy cutoff from which the spacecraft potential is estimated. The spacecraft potential and spacecraft velocity are corrected when computing ion moments. The dashed lines in Figure 2g show the crustal magnetic field computed from the spherical harmonic model [*Morschhauser et al.*, 2014].

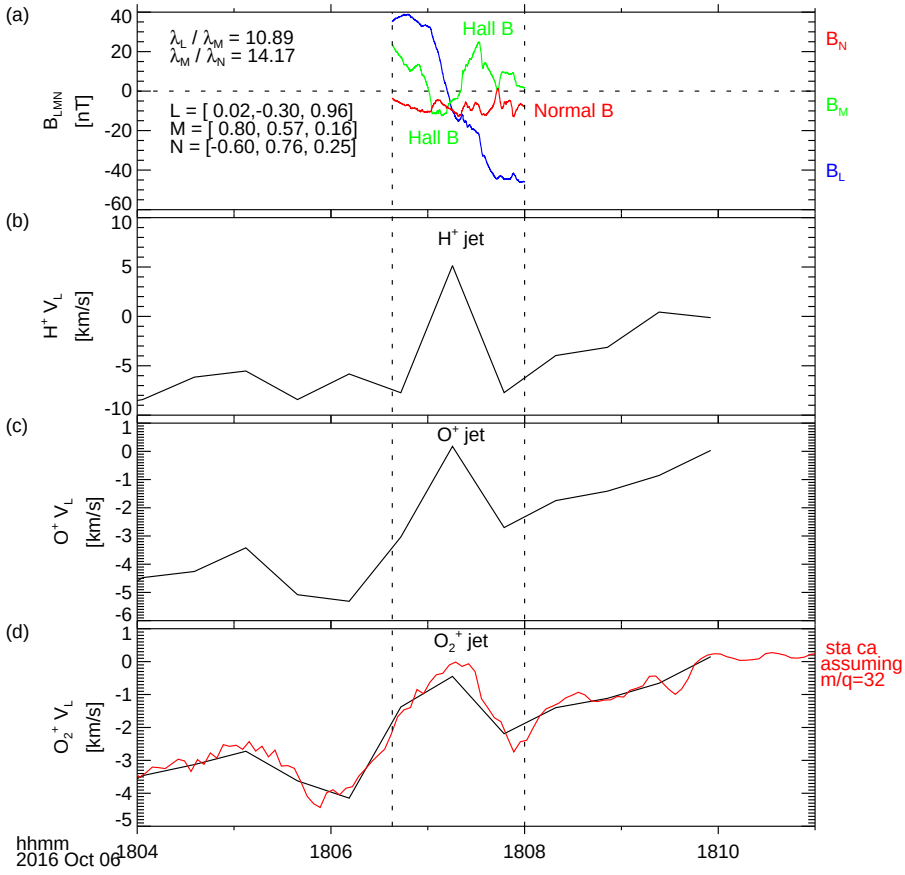

Figure 3. (a) Magnetic fields in the current sheet LMN coordinates, and L component of (b) H^+, (c) O^+, (d) O_2^+ ion velocities. The MVA eigenvalue ratios and the maximum (L), intermediate (M), and minimum (N) variance directions in MSO are noted in Figure 3a. The red line in Figure 3d shows the ion velocity component computed from the high-time resolution, three dimensional data product without mass resolution ("CA" data product, see *McFadden et al.* [2015]) by assuming that all ions are the dominant species, i.e., O_2^+.

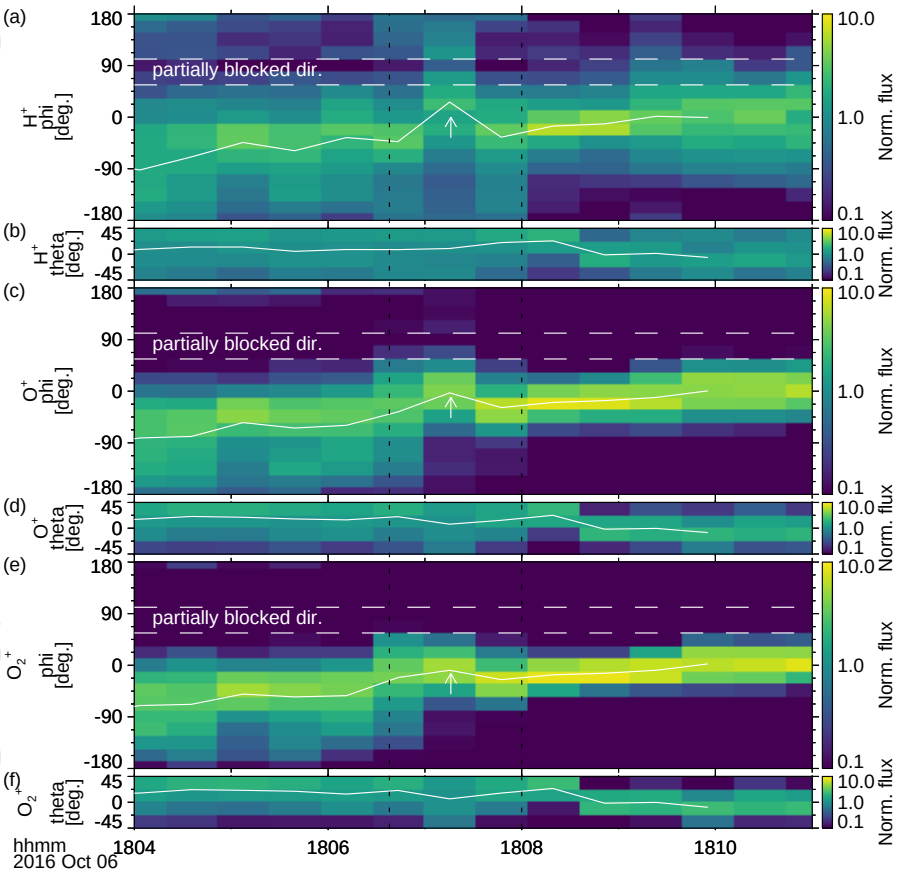

Figure 4. Angular spectra of (a) H^+ in the instrument azimuthal (phi) angle, (b) H^+ in the instrument elevation (theta) angle, (c) O^+ in phi, (d) O^+ in theta, (e) O_2^+ in phi, and (f) O_2^+ in theta. The solid white lines indicate the directions of the computed bulk velocities. The horizontal dashed lines in Figures 4a, 4c, and 4e mark the look directions that were partially blocked by the spacecraft body.